Model of inertial spreading and imbibition of a liquid drop on a capillary plate

Michel Y. Louge* and Shilpa Sahoo

Sibley School of Mechanical and Aerospace Engineering, Cornell University, Ithaca, NY 14853 USA

E-mail: Michel.Louge@cornell.edu

Abstract

We outline a low-order Lagrangian model for the inertial dynamics of spreading and imbibition of a spherical liquid cap on a plane featuring independent cylindrical capillaries without gravity. The analysis predicts the relative roles of radial and axial kinetic energy, reveals the critical Laplace number beyond which the drop oscillates, and attributes the exponent of the initial power-law for contact patch radius vs time to the form of capillary potential energy just after the water sphere touches the plate.

Keywords

capillarity, liquid imbibition, contact angle, liquid spreading, surface tension

Introduction

Spreading and imbibition of a liquid on a porous plane are ubiquitous in printing, cleaning, flooding and irrigation.[1] They begin with an inertial phase that determines how long

a deposited drop rests on a perforated surface before penetrating it, thereby making a hydrophilic solid behave initially as a hydrophobic one. Research on spreading showed that, when a liquid sphere of radius R_0 touches a flat plate, the radius r_c of the contact patch initially grows as a power of time t,

$$\frac{r_c}{R_0} \simeq C\left(\frac{t}{\tau}\right)^{\alpha}, \tag{1}$$

where C is a constant of order unity, and $\tau \equiv \left(\rho R_0^3/\gamma_{\ell g}\right)^{1/2}$ is an inertial "Rayleigh" time scale constructed with fluid density ρ and gas-liquid interfacial energy $\gamma_{\ell g}$. Scaling arguments borrowed from the coalescence of liquid drops[2,3] and experiments[4] imply that $\alpha \simeq 1/2$. However, α decreases with increasing effective contact angle, in a manner that is justified by total energy conservation and initial self-similar growth of the contact patch at the speed of local capillary waves.[5]

Inspired by Denesuk, et al,[6] Frank, Perré and Li[7,8] considered a simpler porous medium consisting of cylindrical unconnected capillaries reminiscent of the structure of wood. During the inertial phase, their Lattice-Boltzmann numerical simulations showed that the permeable surface produced a power law similar to spreading alone, but featuring an exponent α decreasing with the effective Cassie-Baxter (CB) angle[9] of the triple gas-solid liquid contact line. Our recent microgravity experiments[10] concurred with these results. In addition, our statistical mechanics of the contact angle explained why the unconnected capillaries of Frank, et al[7,8] had to conform to CB behavior, which is one of six possible regimes of the contact angle on rough surfaces.[11]

To generate useful predictions, numerical simulations are employed to capture details, such as the flow near the singular moving contact line.[12] Meanwhile, models of spreading and imbibition provide further insight into the roles of inertia, viscous dissipation and capillary forces by describing the dynamics of the entire drop with differential equations. However, these models are burdened by complexity of a flow field that is coupled with the

porous medium below the drop. Therefore, existing models have so far focused on the competition between viscous spreading and capillary penetration,[13,14] or they have ignored initial accelerations when the liquid sphere first spreads on the plate.[15]

In this context, we derive a minimal low-order Lagrangian model for the dynamics of a spreading and imbibing drop, which begins as soon as a liquid sphere touches a plane featuring cylindrical capillaries. For tractability, we regard the drop kinematics as that of a deforming spherical cap. An advantage of such simplification is that geometry and interface potential energy are known exactly, while good approximations can be derived for overall kinetic energy and viscous dissipation at the contact patch. However, as this article will show, the formulation of interface potential energy must be repaired to yield a power-law in Eq. (1) consistent with $\alpha \lesssim 1/2$.

The model is meant for inertial drops at Bond numbers $\rho g R_0^2/\gamma_{\ell g} \ll 1$ for which gravitational acceleration g is unimportant. It serves as a guide for designing future microgravity experiments of drop spreading on capillary plates, which we first tested at the ZARM free-fall tower[10] with relatively large liquid spheres. A challenge in comparing such experiments to numerical simulations is that their Laplace number

$$\mathrm{La} \equiv \rho \gamma_{\ell g} R_0/\mu^2, \tag{2}$$

a kind of Reynolds number based on capillary speed $\gamma_{\ell g}/\mu$, is much larger than what existing Lattice-Boltzmann simulations normally muster,[7,8] thereby raising the question whether large drops of small viscosity μ, such as water, can be simulated in this way. To inform this question, we report here a linear stability analysis around the equilibrium contact angle that reveals a critical Laplace above which the contact patch oscillates.

Despite its limitations, our model is instructive in predicting the onset of drop oscillations, and in revealing the relative importance of terms in the dynamical equation during the inertial phase. We begin with a kinematic description having the instantaneous contact

angle θ as the only time-dependent variable. In the Lagrangian framework, we then derive integral expressions for kinetic energy, interface potential and viscous dissipation. Having posed the resulting dynamical equation, we expand the solution at initial contact ($\theta = \pi$) and around the equilibrium angle ($\theta = \theta_e$). Finally, we outline implications of the model for drop spreading and imbibition.

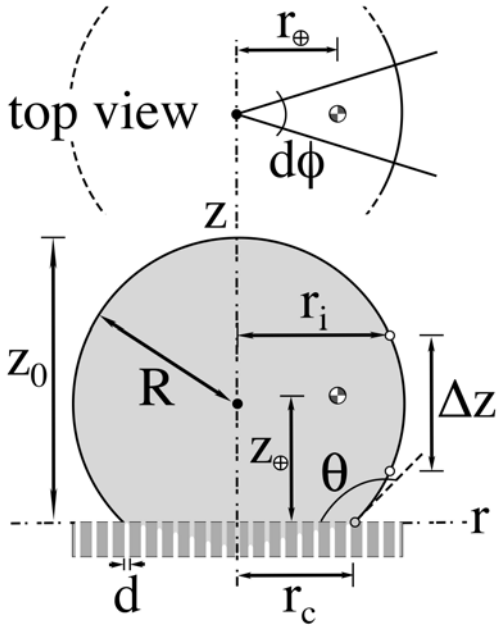

Figure 1: Geometry and symbols, sketched for $\theta = 3\pi/4$.

Kinematics

We consider the liquid drop as an axisymmetric spherical cap spreading on a plane with contact angle $0 < \theta \leqslant \pi$ and patch radius r_c (Fig. 1). When the drop first touches the plane, it is a perfect sphere of radius R_0 with $\theta = \pi$. As it imbibes into capillaries, the volume of liquid above the plane is reduced to $(4/3)\pi R_i^3$ with $R_i \leqslant R_0$, but the drop remains a spherical cap of radius R. In the cap, distances are made dimensionless with R_i and denoted by an asterisk. Symmetry suggests a cylindrical coordinate system with axial distance z along the drop axis perpendicular to the plane. Because interface potential energy is a function of

contact angle cosines,[11] it is convenient to express geometrical variables in terms of $\xi \equiv \cos\theta$. Then, the radii of the cap and the liquid-gas interface radial distance at z are, respectively,

$$R^* \equiv R/R_i = 2^{2/3}/\left(2 - 3\xi + \xi^3\right)^{1/3}, \tag{3}$$

and

$$r_i^* \equiv r_i/R_i = R^*\left[1 - (\xi + z^*/R^*)^2\right]^{1/2}, \tag{4}$$

such that the contact patch radius is

$$r_c^* = r_i^*(z = 0) = R^*\left(1 - \xi^2\right)^{1/2}, \tag{5}$$

At the radial distance r, the drop has thickness Δz along z,

$$\Delta z^* \equiv \Delta z/R_i = R^* \times \begin{cases} 2\left[1 - (r^*/R^*)^2\right]^{1/2} & \text{if } r^* > r_c^* \\ \left[1 - (r^*/R^*)^2\right]^{1/2} - \cos\theta & \text{otherwise,} \end{cases} \tag{6}$$

whereby $z^*(r = 0) \equiv z_0^* = R^*(1 - \cos\theta)$ at the drop apex. In the next section, we will follow the dynamics of a slice of sector $d\phi$ (Fig. 1, top). Its center of gravity, denoted by the subscript $\oplus$, has elevation

$$z_\oplus^* \equiv z_\oplus/R_i = \frac{(1-\xi)^{1/3}(3+\xi)}{2^{4/3}(2+\xi)^{4/3}}, \tag{7}$$

and radial distance from the symmetry axis

$$r_\oplus^* \equiv r_\oplus/R_i = \frac{3\theta - \xi(1-\xi^2)^{1/2}(5-2\xi^2)}{2^{4/3}(1-\xi)^{8/3}(2+\xi)^{4/3}}. \tag{8}$$

As it spreads, the spherical cap has significant velocity components along the radial and axial directions. For simplicity, we evaluate their respective average magnitude $\bar{u}_r$ and $\bar{u}_z$ separately. This integral method is what others have invoked to find $\bar{u}_r$ in the later stage of spreading.[15,16] Neglecting imbibition, volume conservation in a cylindrical shell of height Δz

and elementary thickness dr implies

$$\frac{\partial \Delta z}{\partial t} = -\frac{\partial \left(\bar{u}_r r \Delta z\right)}{r \partial r}, \tag{9}$$

with, by symmetry, $\bar{u}_r \equiv 0$ at $r = 0$. Because R_i can change, but R_0 does not, it is convenient to make time and speed dimensionless with the Rayleigh time τ and R_0/τ, respectively. We denote these relative quantities with a dagger, $t^\dagger$ and $\bar{u}_r^\dagger$. We integrate Eq. (9) from the centerline to any radius r. In dimensionless form,

$$\bar{u}_r^\dagger = -R_i^\dagger \, \dot{\theta} \, \mathbb{I}_r / [r^* \Delta z^*], \tag{10}$$

where $R_i^\dagger \equiv R_i/R_0$, $\dot{\theta} \equiv \partial\theta/\partial t^\dagger$,

$$\mathbb{I}_r \equiv \int_0^{r^*} \frac{\partial \Delta z^*}{\partial \theta} r' \mathrm{d}r' = \begin{cases} \frac{8(1+\xi)^{3/2}\sqrt{1-r^{*2}[(2-3\xi+\xi^3)/4]^{2/3}}}{(2+\xi)^2(1-\xi)^{5/2}} & \text{if } r^* > r_c^* \\ \frac{2^{2/3}(1+\xi)^{1/2}}{(1-\xi)^{7/6}(2+\xi)^{4/3}}\left[r^{*2} + \frac{2^{4/3}(A_1-1)(1+\xi)}{(2+\xi)^{2/3}(1-\xi)^{4/3}}\right] & \text{otherwise,} \end{cases} \tag{11}$$

and $A_1 \equiv [1 - r^{*2}(1-\xi)^{4/3}(2+\xi)^{2/3}/2^{4/3}]^{1/2}$.

In the axial direction, volume conservation for the mean velocity in a wafer of thickness dz implies $\partial r^2/\partial t = -\partial(r^2 \bar{u}_z)/\partial z$. Without imbibition, we integrate this equation subject to $\bar{u}_z = 0$ at $z = 0$ and find the mean dimensionless speed in the axial direction

$$\bar{u}_z^\dagger = -R_i^\dagger \, \dot{\theta} \, \mathbb{I}_z / r_i^{*2}, \tag{12}$$

where

$$\mathbb{I}_z \equiv \int_0^{z^*} \frac{\partial r_i^{*2}}{\partial \theta} \mathrm{d}z' = -\frac{2^{5/3} z^* (1+\xi)^{1/2} [2^{2/3}(1-\xi)^{1/3} - z^*(2+\xi)^{1/3}]}{(2+\xi)^{5/3}(1-\xi)^{7/6}}. \tag{13}$$

Dynamics

For this problem with single time-dependent variable θ, two components of kinetic energy, known interface potential energy, and viscous dissipation, it is natural to invoke the Lagrangian formulation of the equation of motion,

$$\frac{\mathrm{d}}{\mathrm{d}t}\left(\frac{\partial \mathcal{L}}{\partial \dot{\theta}}\right) - \frac{\partial \mathcal{L}}{\partial \theta} = -\frac{\partial \mathcal{D}}{\partial \dot{\theta}}, \tag{14}$$

with Lagrangian $\mathcal{L} = \mathcal{K} - \mathcal{G}$, kinetic energy $\mathcal{K}$, interface potential energy $\mathcal{G}$, and energy dissipation rate $\mathcal{D}$. In this section, we evaluate each of these terms to transform Eq. (14) into an ordinary differential equation for the dynamics of the slice of sector $\mathrm{d}\phi$ (Fig. 1, top) with elementary mass $\mathrm{d}m = \rho(2/3)R_i^3\mathrm{d}\phi$. We calculate energies in $\mathrm{d}\phi$, and report them as dimensionless ratios with $\gamma_{\ell g}R_0^2$ denoted with a dagger†.

Kinetic energy

To a good approximation, the radial component $\mathcal{K}_r$ of the kinetic energy integrates elementary contributions from each cylindrical shell of mass $\mathrm{d}m = \rho r\mathrm{d}r\Delta z\mathrm{d}\phi$ with mean radial velocity in Eq. (10),

$$\mathcal{K}_r^\dagger = \frac{1}{2}R_i^{\dagger 5}\dot{\theta}^2\int_0^{r_m^*}\frac{\mathbb{I}_r^2}{r'\Delta z^*}\mathrm{d}r', \tag{15}$$

where r_m^* is the largest radial distance of the interface, equal to R^* for $\theta > \pi/2$ and r_c^* otherwise. Unfortunately, we cannot find an analytical expression for the integral in Eq. (15). Instead, we turn to a simpler calculation treating the slice as a point mass with position in Eq. (8). Differentiating the latter, we find the radial kinetic energy

$$\mathcal{K}_r^\dagger \simeq \frac{1}{2}\left(\frac{2}{3}R_i^{\dagger 5}\right)\dot{\theta}^2\left(\frac{\partial r_\oplus^*}{\partial \theta}\right)^2 \equiv R_i^{\dagger 5}\dot{\theta}^2\mathcal{F}_r. \tag{16}$$

Numerical integration of Eq. (15) and its approximation in Eq. (16) both vanish at $\theta = \pi$. As Fig. 2 shows, Eq. (16) is sufficiently accurate elsewhere.

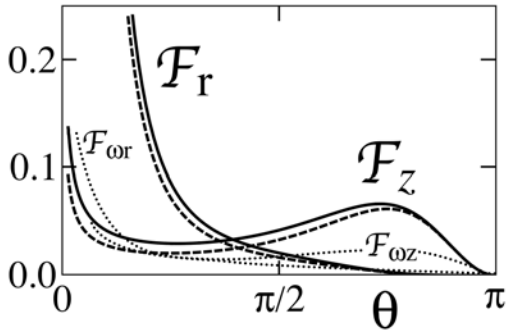

Figure 2: $\mathcal{F}_r$ and $\mathcal{F}_z$ vs θ. Solid lines correspond to a numerical integration of $\mathcal{F}_r$ in Eq. (15) or to the exact result for $\mathcal{F}_z$ in Eq. (18). Dashed line are respective approximations $(1/3)\left(\partial r^*_\oplus/\partial\theta\right)^2$ and $(1/3)\left(\partial z^*_\oplus/\partial\theta\right)^2$. $\mathcal{F}_z > \mathcal{F}_r$ for $\theta \gtrsim 1.28$. Dotted lines are the smaller rotational contributions $\mathcal{F}_{\omega r}$ and $\mathcal{F}_{\omega z}$ in Eqs. (19)–(20).

In the z-direction, a similar calculation yields the axial contribution of each wafer of thickness $\mathrm{d}z$ and mass $\mathrm{d}m = \rho(r_i^2/2)\mathrm{d}z\mathrm{d}\phi$ to the kinetic energy. In dimensionless form, this integral from base at $z = 0$ to apex at $z^* = z_0^*$ is

$$\mathcal{K}_z^\dagger = \frac{1}{4}R_i^{\dagger 5}\dot\theta^2\int_0^{z_0^*}\frac{\mathbb{I}_z^2}{r_i^{*2}}\mathrm{d}z' = R_i^{\dagger 5}\dot\theta^2\mathcal{F}_z, \tag{17}$$

which integrates to

$$\mathcal{F}_z = \frac{8\times 2^{1/3}(1+\xi)}{(1-\xi)^{13/3}(2+\xi)^{11/3}}\left\{2\ln 2 - \frac{4}{3} + \xi\left[4\ln 2 - 1 + 2\xi\,(1+\ln 2) + \frac{\xi^2}{3}\right] - 2\,(1+\xi)^2\ln(1+\xi)\right\}. \tag{18}$$

Like Eq. (16), this exact expression is close to an estimate of the axial kinetic energy $\mathcal{K}_z^\dagger \simeq (1/3)R_i^{\dagger 5}\dot\theta^2(\partial z_\oplus/\partial\theta)^2$ that treats the drop as a point concentrated on its center of mass.

Finally, the drop is subject to rotational kinetic energy $\simeq \mathcal{K}_{\omega r}^\dagger + \mathcal{K}_{\omega z}^\dagger \equiv R_i^{\dagger 5}\dot\theta^2(\mathcal{F}_{\omega r} + \mathcal{F}_{\omega z})$ (dotted lines in Fig. 2), since the radial and axial velocity estimates $\bar u_r$ and $\bar u_z$ at every point (Eqs. 10 and 12) do not always intersect the slice's center of mass. We estimate their respective contributions numerically as

$$\mathcal{F}_{\omega r} = \int_0^{r_m^*}\int_{\Delta z^*}\frac{1}{2}\|\mathbf{r}^* - \mathbf{r}^*_\oplus\|^2\left(\frac{\|(\mathbf{r}^* - \mathbf{r}^*_\oplus)\times\bar{\mathbf{u}}_r\|}{\|\mathbf{r}^* - \mathbf{r}^*_\oplus\|^2}\right)^2 r'\mathrm{d}r'\mathrm{d}z' \tag{19}$$

and

$$\mathcal{F}_{\omega z} = \int_0^{z_0^*} \int_0^{r_i^*} \frac{1}{2} \|\mathbf{r}^* - \mathbf{r}_\oplus^*\|^2 \left(\frac{\|(\mathbf{r}^* - \mathbf{r}_\oplus^*) \times \bar{\mathbf{u}}_z\|}{\|\mathbf{r}^* - \mathbf{r}_\oplus^*\|^2} \right)^2 r' \mathrm{d}r' \mathrm{d}z' \tag{20}$$

In these expressions, we assume for simplicity that the radial velocity is everywhere equal to $\bar{u}_r^*$; boldface $\mathbf{r}^*$ denote vector positions of elements $r^* \mathrm{d}r^* \mathrm{d}z^* \mathrm{d}\phi$; and the integration over Δz^* in Eq. (19) is meant across the thickness of the drop at the radial distance r'. As Fig. 2 shows, rotational kinetic energy is smaller than the sum of its translational counterparts by at least a factor of three. Because it has negligible effects on drop dynamics, we ignore it to adopt closed-form expressions as much as possible.

Potential energy

To calculate the energy barrier responsible for pinning a line having a hysteretic contact angle, and to provide *ab initio* predictions for the latter's advancing and receding values, Louge[11] recently derived an expression for the interface potential energy of a spherical liquid cap (solid line, Fig. 3). For a small change in contact patch area that arises from a variation in θ, the corresponding potential change of a slice of sector $\mathrm{d}\phi$ is $\partial \mathcal{G}/\partial\theta = \gamma_{\ell g}(\xi - \xi_e) r_c \partial r_c/\partial\theta$, where $\xi_e \equiv \cos\theta_e$ is the cosine of the equilibrium contact angle θ_e; in dimensionless form,

$$\frac{\partial \mathcal{G}^\dagger}{\partial \theta} = R_i^{\dagger 2} (\xi - \xi_e) r_c^* \frac{\partial r_c^*}{\partial \theta} \equiv R_i^{\dagger 2} \Phi. \tag{21}$$

Although it is possible to interpret Φ as a line force restoring contact line equilibrium, such concept may be less fruitful to a dynamical simulation, since a force applied on a line can lead to artifical distortions of the local flow field. Instead, one may consider the global potential change that a drop experiences, using a Lagrangian framework like Eq. (14).

Dissipation rate

To estimate the energy dissipation rate, we follow Brocard-Wyart and de Gennes[16] and Härth and Schubert[15] and adopt a lubrication approximation to calculate the shear stress

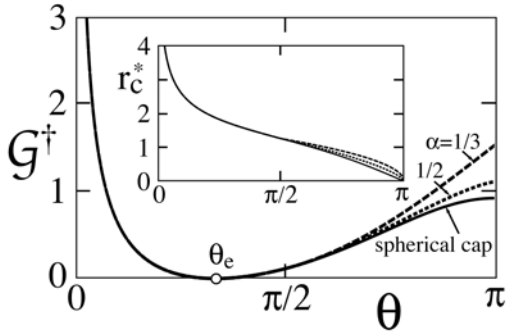

Figure 3: Interface potential energy $\mathcal{G}^\dagger$ vs θ for $\theta_e = \pi/3$. Inset: dimensionless contact patch radius r_c^* vs θ. Solid, dashed and dotted lines represent, respectively, expressions for a spherical cap,[11] and corrections consistent with $\alpha = 1/2$ and $1/3$, respectively.

at the base. Although this approximation is not accurate when θ is large, the error should be of little consequence to the dissipation, since the latter is small at those angles. In this approximation, the radial component of the Navier-Stokes (NS) equation has no inertial terms, the dominant second derivative of u_r is $\partial^2 u_r/\partial z^2$, and the pressure gradient $\partial P/\partial r$ varies negligibly in the z-direction. In this case, the radial NS equation integrates to

$$\frac{u_r}{\bar{u}_r} = 3\frac{z}{\Delta z}\left[1 - \frac{1}{2}\left(\frac{z}{\Delta z}\right)\right], \tag{22}$$

thereby yielding a shear stress on the wetted solid at $z = 0$

$$S_0 = 3\mu\frac{\bar{u}_r}{\Delta z}. \tag{23}$$

The working of this shear force through the mean radial velocity $\bar{u}_r$ of the infinitesimal shell of cross-section area $r\mathrm{d}\phi\mathrm{d}r$ at the radial distance r yields the dissipation rate $\mathrm{d}\mathcal{D} = (1/2)\bar{u}_r S_0 r\mathrm{d}\phi\mathrm{d}r$ in the sector $\mathrm{d}\phi$. Integrating this expression from $r = 0$ to the edge of the contact patch at r_c, making the energy dissipation rate dimensionless with $\gamma_{\ell g}R_0^2/\tau$, and substituting $\bar{u}_r^{\dagger 2}$ using Eq. (10), we find

$$\mathcal{D}^\dagger = \left(\frac{\dot{\theta}^2}{2}\right)\frac{R_i^{\dagger 3}}{\mathrm{La}^{1/2}}\int_0^{r_c^*}\frac{3\mathbb{I}_r^2}{r'\Delta z^{*3}}\mathrm{d}r' \equiv \left(\frac{\dot{\theta}^2}{2}\right)\frac{R_i^{\dagger 3}}{\mathrm{La}^{1/2}}\mathcal{F}_D \tag{24}$$

This dependence of the dissipation rate on $\mathrm{La}^{-1/2}$ explains why viscous damping is a relatively slow process for large liquid drops of low viscosity.

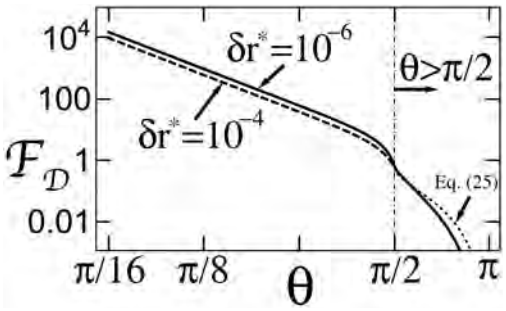

Figure 4: Dissipation coefficient $\mathcal{F}_D$ vs θ. The solid line represents the numerical integration of $\mathcal{F}_D$ in Eq. (24) for $\delta r^* \simeq 10^{-6}$, which corresponds to water spheres staged by Steub, et al[10] at a typical cut-off length of 10 nm;[17] the dashed line is $\delta r^* \simeq 10^{-4}$. For $\theta < \pi/2$, these integrations are very close to Eq. (27). For $\theta > \pi/2$, δr^* no longer matters, dissipation is much smaller, and it is well approximated with Eq. (25) (dotted line).

Unfortunately, we cannot find an analytical expression for the integral $\mathcal{F}_D$ in Eq. (24), and therefore we evaluate it approximately. Because the drop has relatively large Δz for $\theta > \pi/2$, the dissipation rate is small at those angles. Integrating the leading order in a series expansion of the integrand of $\mathcal{F}_D$ yields

$$\mathcal{F}_D(\theta > \pi/2) \simeq 3\ln 2 - \frac{3}{2}(1 - A_2) - 3\ln(1 + A_2)\,, \tag{25}$$

where $A_2 = \sqrt{1 - 2^{2/3}(1+\xi)/[(1-\xi)^{1/3}(2+\xi)^{2/3}]}$. At $\theta = \pi/2$, $\mathcal{F}_D \equiv \mathcal{F}^{\dagger}_{D_0} \simeq 3\ln 2 - 3/2$.

Because the thickness Δz of the liquid wedge vanishes at the contact line for $\theta < \pi/2$, the integral must be regularized for these contact angles, as it is in the singular problem of the moving contact line.[1] We do so by interrupting integration at a small distance δr from the line. Because the integrand of $\mathcal{F}_D$ is inversely proportional to Δz^{*3}, the neighborhood of the contact line dominates it. Then, a series expansion of the integrand for small $\delta r^* \equiv r_c^* - r^*$ reveals the form of the singularity. Using $\Delta z^* \simeq \tan\theta\, \delta r^*$ as $r \to r_c$ and the expression for $\mathbb{I}_r$ for $r^* < r_c^*$ in Eq. (11), we find $3\mathbb{I}_r^2/r^*\Delta z^{*3} \simeq 12\xi/[(1-\xi)^2(2+\xi)^3] \times \delta r^{*-1} + o(\delta^{*0})$, which

integrates to within δr from the contact line as

$$\mathcal{F}_D(\theta < \pi/2) \simeq \frac{12\xi}{(1-\xi)^2(2+\xi)^3}\left[\ln(r_c^*) - \ln(\delta r^*)\right]. \tag{26}$$

As expected, this logarithmic singularity has the same form as that of the moving contact line.[18,19] Patching the two expressions in Eqs. (25)-(26), we approximate the integral as

$$\mathcal{F}_D \simeq \begin{cases} 3\ln 2 - 3/2 + \frac{12\xi}{(1-\xi)^2(2+\xi)^3}\left[\ln(r_c^*) - \ln(\delta r^*)\right] & \text{if } \theta < \pi/2 \\ 3\ln 2 - \frac{3}{2}(1-A_2) - 3\ln(1+A_2) & \text{otherwise.} \end{cases} \tag{27}$$

Figure 4 illustrates the result.

Solution

Collecting terms from Eqs. (3)–(5), (8), and (16)–(21), we write Eq. (14) in dimensionless form as an ordinary differential equation (ODE) for the dynamics of sector $\mathrm{d}\phi$,

$$2(\mathcal{F}_r + \mathcal{F}_z)\left[\dot{\theta}\frac{\mathrm{d}R_i^{\dagger 5}}{\mathrm{d}t^\dagger} + \ddot{\theta}R_i^{\dagger 5}\right] + \dot{\theta}^2 R_i^{\dagger 5}\frac{\partial(\mathcal{F}_r + \mathcal{F}_z)}{\partial\theta} + R_i^{\dagger 2}\Phi + \frac{\mathcal{F}_D}{\mathrm{La}^{1/2}}\dot{\theta}R_i^{\dagger 3} = 0, \tag{28}$$

where each dot denotes the derivative with respect to dimensionless time $t^\dagger$. To model the gentle touch of a liquid sphere on the plane, we integrate this equation numerically subject to $\theta = \pi$ and $\dot{\theta} = 0$ at $t = 0$. Because $\mathcal{F}_r$, $\mathcal{F}_z$, their time derivatives, $\mathcal{F}_D$ and Φ vanish at $\theta = \pi$, we start a Runge-Kutta numerical integration of ODE (28) from a small finite time, at which we evaluate θ by carrying series expansions of these terms in $\delta_\theta \equiv \pi - \theta$.

Inertial spreading at $\theta \lesssim \pi$

Series expansions around $\theta \lesssim \pi$ also determine the power-law for r_c^* at small times without imbibition ($R_i^\dagger = 1$). There, we find $\mathcal{F}_r = (3\pi^2/256)\delta_\theta^6 + o(\delta_\theta^7)$, $\mathcal{F}_z = (1/3)\delta_\theta^2 + o(\delta_\theta^4)$, $\Phi = (1+\xi_e)\delta_\theta + o(\delta_\theta^3)$, and $\mathcal{F}_D = 3\delta_\theta^4/[2^{1/3}\times 64] + o(\delta_\theta^6)$. Substituting in ODE (28) and retaining

only the leading order, we obtain $\dot{\theta} = -\dot{\delta}_\theta = -[3(1+\xi_e)/2]^{1/2}$ or $\delta_\theta \simeq [3(1+\xi_e)/2]^{1/2} t^\dagger$. Because $r_c^* = \delta_\theta + o(\delta_\theta^3)$, Eq. (28) predicts a linear rise of the contact patch radius with time.

Such behavior contradicts experimental evidence[4,20] of an exponent $\alpha \lesssim 1/2$ that decreases with θ_e.[5,7,8] Our analysis suggests that the contribution of the neighborhood of the contact line to the overall interface potential energy is responsible for the discrepancy. In that neighborhood, observations show that the gas-liquid interface exhibits an inward cusp connected smoothly to the nearly spherical drop apex above, but making an angle of contact with the solid plane closer to θ_e than what a perfectly spherical cap would produce.[4,5,7,8,20] By creating extra interface area, the cusp therefore raises the potential $\mathcal{G}$ of the entire drop. Meanwhile, for θ near π, other terms in ODE (28) are unlikely to explain the power-law mismatch: viscous dissipation $\mathcal{F}_D \sim \delta_\theta^4$ is much smaller than $\partial \mathcal{F}_z/\partial\theta \sim \delta_\theta$; axial kinetic energy dominates its radial counterpart, $\mathcal{F}_z \gg \mathcal{F}_r$; and both these integral quantities should be relatively insensitive to the actual form of the velocity field.

In this context, we exploit once again the series expansion around $\theta \lesssim \pi$ to derive a form of the interface potential that is compatible with observations. This expansion suggests that two terms of Eq. (28) are in balance during the early inertial phase when δ_θ is small, namely $\dot{\theta}^2 \partial \mathcal{F}_z/\partial\theta$ and Φ. To capture how the cusp makes the contact patch radius grow faster with δ_θ than linearly, we write $r_c^* = a\delta_\theta^n$, with exponent n to be determined. Ignoring imbibition for now ($R_i^\dagger = 1$), Eq. (21) then yields $\Phi = a^2(1+\xi_e) n \delta_\theta^{2n-1}$. Substituting in ODE (28) and retaining the leading order, we find $\dot{\delta}_\theta \simeq [(3/2) n a^2 (1+\xi_e)]^{1/2} \delta_\theta^{n-1}$. Integrating this ODE for δ_θ in time and substituting in the expression for patch radius, we find $r_c^* \sim a^{2/(2-n)} [(3/2) n (2-n)^2 (1+\xi_e)]^{n/(4-2n)} t^{\dagger n/(2-n)}$. Matching the exponent in Eq. (1) and joining Eq. (5) at $\theta = \pi/2$, we find

$$r_c^* = \begin{cases} R^* \left(1-\xi^2\right)^{1/2} & \text{if } \theta < \pi/2 \\ 2^{(1+7\alpha)/[3(1+\alpha)]} \left(1-\theta/\pi\right)^{2\alpha/(1+\alpha)} & \text{otherwise.} \end{cases} \tag{29}$$

Although this expression for r_c^* is hardly larger than Eq. (5), it yields an interface potential

derivative that is now consistent with the power law in Eq. (1),

$$\Phi = (\xi - \xi_e) \times \begin{cases} r_c^* \partial r_c^* / \partial \theta & \text{if } \theta < \pi/2 \\ -2^{4(2\alpha-1)/[3(1+\alpha)]} \left(1 - \theta/\pi\right)^{(3\alpha-1)/(1+\alpha)} & \text{otherwise,} \end{cases} \tag{30}$$

and an interface potential for $\pi/2 < \theta < \pi$ than is slightly higher at $\theta \lesssim \pi$ than what Louge had calculated,[11]

$$\mathcal{G}^\dagger(\theta > \pi/2) = -\frac{2^{2/3}\pi}{\alpha \times 2^{\frac{4}{(1+\alpha)}}}(1-\theta/\pi)^{\frac{4\alpha}{(1+\alpha)}}\left[(1+\alpha)\xi_e - 2\alpha\mathbb{C}_m(\pi-\theta)\right] \tag{31}$$
$$-2^{1/3}(1-\xi_e)^{2/3}(2+\xi_e)^{1/3} + (2-\xi_e)/2^{1/3} + \frac{\pi}{8\times 2^{1/3}\alpha}\left[(1+\alpha)\xi_e - 2\alpha\mathbb{C}_m(\pi/2)\right],$$

where $\mathbb{C}_m(\beta) \equiv \int_1^\infty 2\cos(\beta x)/x^m dx = E_m(-\imath\beta) + E_m(+\imath\beta)$, $\imath^2 = -1$, $E_m(z)$ is a converging integral function called `ExpIntegralE` in MATHEMATICA, and $m = (1-3\alpha)/(1+\alpha)$.

A definitive model remains to be derived for the inertial flow field around the contact patch as a drop first touches a plane.[17] Analyses of the inner solution near the contact line[20] would be particularly fruitful to explain the seemingly universal nature of the power-law,[4] and to derive how its exponent varies with equilibrium contact angle.[5] If such solution can be found, the corresponding potential should be given by Eq. (31).

Near equilibrium

We now examine ODE (28) when θ is near its equilibrium value θ_e, without imbibition. Because θ is now far from π in most practical cases, we adopt the potential derivative Φ in Eq. (21) with r_c^* from Eq. (5). First, we expand the governing equation in small $\delta_e \equiv \theta - \theta_e$,

$$\ddot{\delta_e} \simeq -\mathcal{F}_\Theta \dot{\delta_e}^2 - \mathcal{F}_\Phi \delta_e - \mathcal{F}_\Delta \dot{\delta_e}/\mathrm{La}^{1/2}, \tag{32}$$

where $\mathcal{F}_\Theta \equiv (1/2)\partial \ln\left(\mathcal{F}_r + \mathcal{F}_z\right)/\partial\theta$ and $\mathcal{F}_\Delta \equiv \mathcal{F}_D/[2\left(\mathcal{F}_r + \mathcal{F}_z\right)]$ are evaluated at θ_e, and $\mathcal{F}_\Phi = (3/2)(2+\xi_e)^3/\{1 + (1+\xi_e)^2[3\theta_e - (4-\xi_e)(1-\xi_e^2)^{1/2}]^2/(1-\xi_e)^6\}$ is the leading order

of a series expansion of $\Phi/[2\,(\mathcal{F}_r + \mathcal{F}_z)]$ at small δ_e. Then, seeking solutions of the form $\delta_e = \delta_0 \exp(\imath s^\dagger t^\dagger)$ with $\imath^2 = -1$, we note that the term in $\mathcal{F}_\Theta$ is of order δ_0^2 and thus can be neglected. The remaining terms yield the characteristic equation $s^{\dagger 2} - \mathcal{F}_\Delta \imath s^\dagger / \mathrm{La}^{1/2} - \mathcal{F}_\Phi = 0$, which has two roots $s^{\dagger\pm} = \imath \mathcal{F}_\Delta / [2\mathrm{La}^{1/2}] \times [1 \pm (1 - \mathrm{La}/\mathrm{La}_c)^{1/2}]$, with critical Laplace number

$$\mathrm{La}_c = \mathcal{F}_\Delta^2 / [4\mathcal{F}_\Phi]. \tag{33}$$

For small $\mathrm{La} < \mathrm{La}_c$, the equilibrium returns as $\exp(-t^\dagger / t_\pm^\dagger)$ on times $t_\pm^\dagger \equiv 2\mathrm{La}^{1/2}/\mathcal{F}_\Delta/[1 \pm (1 - \mathrm{La}/\mathrm{La}_c)^{1/2}]$. However, at larger $\mathrm{La} > \mathrm{La}_c$, which we expect for relatively large drops of water, the contact line oscillates around its equilibrium position as $\exp(-t^\dagger \mathcal{F}_\Delta / [2\mathrm{La}^{1/2}]) \exp(\imath 2\pi f^\dagger t^\dagger)$ at a dimensionless frequency $f^\dagger = \mathcal{F}_\Delta / [4\pi \mathrm{La}^{1/2}](\mathrm{La}/\mathrm{La}_c - 1)^{1/2}$.

As with numerical simulations,[7,8] this calculation is predicated on a contact angle without hysteresis. However, if the latter was substantial, a potential energy barrier between contact angle advance and recession[11] would pin the contact line and prevent it from ebbing and flowing at $\mathrm{La} > \mathrm{La}_c$. In that case, the natural oscillations at large Laplace number would result in deformations of the drop away from the simple spherical cap. This is what we observed in our own microgravity experiments with $\mathrm{La} \simeq 6.10^5$, where oscillations at the pinned contact line swayed the interface back and forth from receding to advancing angles.[10]

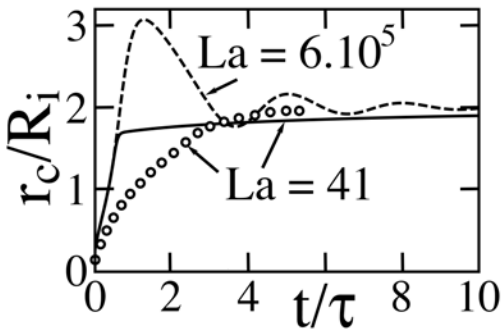

Figure 5: Spreading of the dimensionless contact patch radius r_c^* vs inertial time $t^\dagger$ for the conditions in the numerical simulations of Frank and Perré[7] (symbols) with La = 41.3, $\theta_e = 36^\circ$ and $\alpha = 0.553$. The solid line is the corresponding prediction of ODE (28) with dissipation cutoff $\delta r^* = 10^{-6}$. The dashed line is for $\mathrm{La} = 6\,10^5$, which is beyond the critical $\mathrm{La}_c \simeq 17,000$ in Eq. (33) at this equilibrium contact angle.

An important consequence of Eq. (33) is that the critical Laplace number decreases sharply with contact angle. For instance, Eq. (33) predicts $\mathrm{La}_c \propto \theta_e^{-4.79\pm0.01}$ for $0 \lesssim \theta_e \lesssim 1$. The decline of La_c is even sharper at hydrophobic θ_e, as it reflects the rapid downtrend of $\mathcal{F}_D$ with contact angle in Fig. 4. Therefore, hydrophobic surfaces are more prone to oscillations that hydrophilic ones.

Figure 5 compares the solution of ODE (28) with numerical simulations of Frank and Perré[7] at a small $\mathrm{La} \simeq 41$, and illustrates how raising this number beyond its critical La_c induces oscillations of the contact patch radius. The model overpredicts how rapidly this radius reaches its asymptotic value $r_e^* \equiv r_c^*(\theta_e)$. This suggests that the kinetic energy coefficients $\mathcal{F}_z$ and $\mathcal{F}_r$ are underpredicted by the estimates in Eqs. (15)–(20), and that a more complicated derivation of the flow field is necessary.

Imbibition

We now couple liquid imbibition and drop spreading. To do so, we let R_i change as the drop penetrates cylindrical capillaries of diameter d arrayed on the plane at a surface fraction ϵ. We assume that the flow in each capillary has reached its asymptotic speed $[\gamma_{\ell g} d \cos\theta_e/(16\mu t)]^{1/2}$ when fluid inertia ceases to matter.[21–23] Without gravity, this is typically achieved after a time $\sim \rho d^2/(8\mu)$ or, in dimensionless form, for $t^\dagger \gtrsim t_c^\ddagger = \mathrm{La}^{1/2}(d/R_0)^2/8$. With this simplification, the rate of volume imbibition is given by

$$-\frac{4}{3}\pi\frac{\mathrm{d}R_i^3}{\mathrm{d}t} = \epsilon\left(\frac{\gamma_{\ell g} d\cos\theta_e}{16\mu}\right)^{1/2}\int_{r=0}^{r_c}\frac{2\pi r\mathrm{d}r}{\sqrt{t-t_r}}, \tag{34}$$

where t_r is when the triple contact line of radius r_c reached the radial distance r and begun imbibing at the asymptotic capillary speed.

If, as expected, the contact patch radius initially rises as a power-law, then $t_r/t = (r/r_c)^{1/\alpha}$. However, this growth cannot proceed indefinitely. For the sole purpose of evaluating the integral in Eq. (34), we assume for simplicity that the radius saturates at its equilibrium

value r_e^* at a time $t_e^\dagger = (r_e^*/C)^{1/\alpha}$. Then, for $t^\dagger > t_e^\dagger$, $t_r/t = (t_r/t_e) \times (t_e/t) = (r^*/r_e^*)^{1/\alpha} \times (t_e^\dagger/t^\dagger)$. In dimensionless form, Eq. (34) becomes

$$\frac{\mathrm{d}R_i^\dagger}{\mathrm{d}t^\dagger} = -\frac{\epsilon}{8}\left(\frac{d}{R_0}\right)^{1/2}\left[\frac{\mathrm{La}^{1/2}\cos\theta_e}{t^\dagger}\right]^{1/2}\mathbb{I}, \tag{35}$$

where

$$\mathbb{I} = \left\{ \begin{array}{l} r_c^{*2}\int_0^1 \frac{r'\mathrm{d}r'}{\sqrt{1-r'^{1/\alpha}}} \\ r_e^{*2}\int_0^1 \frac{r'\mathrm{d}r'}{\sqrt{1-\frac{t_c^\dagger}{t^\dagger}r'^{1/\alpha}}} \end{array} \right\} = \left\{ \begin{array}{ll} r_c^{*2}\times\alpha\pi^{1/2}\Gamma(2\alpha)/\Gamma(2\alpha+1/2) & \text{if } t^\dagger < t_e^\dagger \\ r_e^{*2}\times {}_2F_1\left(\frac{1}{2}, 2\alpha; 1+2\alpha; t_e^\dagger/t^\dagger\right)/2 & \text{otherwise} \end{array} \right\}, \tag{36}$$

and Γ and ${}_2F_1$ are Gamma and Hypergeometric functions, respectively.

As the simulations of Frank, Perré and Li[8] and our microgravity experiments[10] showed, the contact angle presented by the perforated plane is the effective Cassie-Baxter angle

$$\cos\theta_e^{\mathrm{CB}} = (1-\epsilon)\cos\theta_e - \epsilon, \tag{37}$$

which corresponds to "regime VI" for unconnected surface cavities.[11] Therefore, with a perforated surface, $\cos\theta_e^{\mathrm{CB}}$ should replace θ_e wherever it appears earlier, including r_e^*, but not in Eqs. (34)–(35), which concern flow in capillaries. As Fig. 6 shows, the model supports this. Although it predicts a drop height falling too early, the model implies a critical Laplace number $\mathrm{La}_c \simeq 2$ with $\cos\theta_e^{\mathrm{CB}}$ below the value of 41.3 staged by Frank and Perré,[7] which likely explains oscillations in their drop height (Fig. 6). In contrast, if the capillary surface behaved with its nominal contact angle θ_e, these oscillations would disappear (dashed lines).

When imbibition takes place, the mean axial velocity $\bar{u}_{z0}^\dagger$ does not vanish at the capillary plate where $z = 0$. In this case, the expression in Eq. (12) becomes $r_i^{*2}\bar{u}_z^\dagger = r_c^{*2}\bar{u}_{z0}^\dagger - R_i^\dagger\,\dot{\theta}\,\mathbb{I}_z$, where $r_c^{*2}\bar{u}_{z0}^\dagger = 4\mathrm{d}R_i^\dagger/\mathrm{d}t^\dagger$ by volume conservation, and the expression for $\mathcal{K}_z^\dagger$ is more complicated than Eqs. (17)-(18). The form of Eq. (35) suggests when this difficulty can be ignored at long times, or at small Laplace number, surface fraction, or capillary diameter

relative to R_0. Such is the case, for example, in the simulations of Frank and Perré, where $(\epsilon/2)(d/R_0)^{1/2}\mathrm{La}^{1/4}\cos^{1/2}\theta_e^{\mathrm{CB}} < 0.04$.

The model predicts an imbibition process that is more rapid than observed in simulations (Fig. 6). While this may be due in part to its hasty spreading of the contact patch (Fig. 5), the model does not explicitly take into account how imbibition is further hampered by a difficult progression of the contact line as it jumps over each individual capillaries.[24]

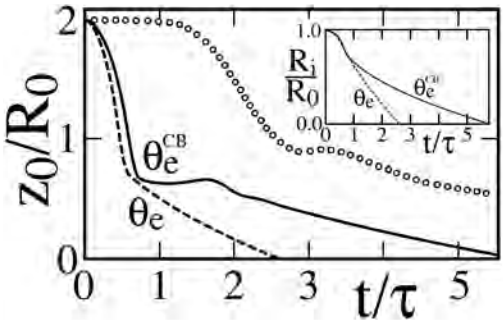

Figure 6: Relative centerline elevation z_0/R_0 vs $t^\dagger$ in simulated imbibition[7] (symbols) for conditions of Fig. 5 and a time $t_c^\dagger \simeq 0.04$ to asymptotic capillary speed. Dashed and solid lines are integrations of Eqs. (28) and (35) for, respectively, equilibrium angles $\theta_e = 36\,^\circ$ and θ_e^{CB} in Eq. (37). At θ_e^{CB}, the critical Laplace number is $\mathrm{La}_c \simeq 2$, while it is $\simeq 17,000$ at θ_e. Inset: predictions of effective drop radius $R_i = [3V/(4\pi)]^{1/3}$ relative to its initial value R_0.

Conclusions

We outlined a Lagrangian analytical model of the spreading of a liquid drop on a plane without contact angle hysteresis or gravity, possibly coupled with imbibition of the liquid into unconnected capillaries. To describe the early phase of spreading, which had hitherto eluded dynamical modeling,[13–15] a closed-form analysis was made tractable by invoking the common simplification that the drop remains shaped as a spherical cap, and by ignoring obstructions that individual capillaries present to the advancing contact line.[24]

Although comparisons with numerical simulations[7,8] suggested that kinetic energy is underpredicted, our analysis showed that the axial component of this energy governs the initial rate of spreading, while its radial counterpart begins to dominate as the contact angle

falls below $\theta \simeq 1.3$. Our analysis also explained why the contact angle oscillates about its equilibrium θ_e for Laplace numbers above a critical value La_c. Because La_c decreases sharply as θ_e rises, we predicted that hydrophobic solid surfaces are more prone to such oscillations. If these surfaces featured unconnected capillaries, we showed that their effective equilibrium angle would rise with hole surface fraction, therefore becoming more hydrophobic than the bare solid, consistent with theory[9,11] and with numerical[8] and experimental[10] observations that the effective Cassie-Baxter angle is the relevant parameter governing the power law in Eq. (1). In this context, we suggested that fluctuations in patch radius and drop height seen in simulations are due to sharp reductions in La_c arising from an effective angle that is higher than θ_e on the bare solid.

Failure of the model to reproduce the observed exponent in the power law[4,5,7,8,20] suggested that the spherical cap assumption produces a contact line potential that must be repaired in the early inertial phase of spreading. Here, the model was instructive in prescribing the form that this potential must take (Eqs. 30–31).

Because a finite Bond number $\mathrm{Bo} = \rho g R_0^2/\gamma_{\ell g}$ would distort the spherical cap[25] and undermine our closed-form expressions, this analytical model was only meant for low gravity. However, because the contact angle does not depend on Bo,[26] the model might qualitatively predict oscillations near the equilibrium contact angle at low Bo by adding a new term $(2/3)\mathrm{Bo}R_i^{\dagger 4} z_\oplus^*$ to potential energy $\mathcal{G}^\dagger$ of the sector $\mathrm{d}\phi$.

Overall, despite its simplicity, the model captured qualitative features of spreading and imbibition into unconnected capillaries, and it identified the origin of oscillations that are exacerbated by high effective contact angles of the perforated surface.

Acknowledgement

The authors are grateful to Enrique Ramé, Patrick Perré, Hervé Duval, Jonathan Kollmer and two anonymous reviewers for fruitful suggestions. They feel honored to celebrate Roy

Jackson's accomplishments. This paper was made possible by NPRP Grant No. 6-059-2-023 from the Qatar National Research Fund. SS was supported by NSF Grant CBET 1637531.

References

(1) Bonn D, Eggers J, Indekeu J, Meunier J, Rolley E. Wetting and spreading. *Rev Mod Phys.* 2009; 81:739–805.

(2) Thoroddsen ST, Takehara K, Etoh TG. The coalescence speed of a pendent and a sessile drop. *J Fluid Mech.* 2005; 527:85–114.

(3) Eggers J, Lister JH, Stone HA. Coalescence of liquid drops. *J Fluid Mech.* 1999; 401:293–310.

(4) Stapelbroek BBJ, Jansen HP, Kooij ES, Snoeijer JH, Eddi A. Universal spreading of water drops on complex surfaces. *Soft Matter.* 2014; 10:2641–2648.

(5) Bird JC, Mandre S, Stone HA. Short-time dynamics of partial wetting. *Phys Rev Lett.* 2008; 100:234501.

(6) Denesuk M, Smith G, Zelinski B, Kreidl N, Uhlmann D. Capillary penetration of liquid droplets into porous materials. *J Colloid and Interface Science.* 1993; 158:114 – 120.

(7) Frank X, Perré P. Droplet spreading on a porous surface: A lattice Boltzmann study. *Phys Fluids.* 2012; 24:042101.

(8) Frank X, Perré P, Li HZ. Lattice Boltzmann investigation of droplet inertial spreading on various porous surfaces. *Phys Rev E.* 2015; 91:052405.

(9) Cassie ABD, Baxter S. Wettability of porous surfaces. *Trans Faraday Soc.* 1944; 40:546–551.

(10) Steub L, Kollmer J, Paxson D, Sack A, Pöschel T, Bartlett J, Berman D, Richardson Y, Louge MY. Microgravity spreading of water spheres on hydrophobic capillary plates. *EPJ Web of Conferences*. 2017;140:16001.

(11) Louge MY. Statistical mechanics of the triple contact line. *Phys Rev E*. 2017; 95:032804.

(12) Chamakos NT, Kavousanakis ME, Boudouvis AG, Papathanasiou AG. Droplet spreading on rough surfaces: Tackling the contact line boundary condition. *Phys Fluids*. 2016; 28:022105.

(13) Starov V, Zhdanov S, Kosvintsev S, Sobolev V, Velarde M. Spreading of liquid drops over porous substrates. *Adv Colloid and Interface Science*. 2003; 104:123 – 158.

(14) Davis SH, Hocking LM. Spreading and imbibition of viscous liquid on a porous base. II. *Phys Fluids*. 2000; 12:1646–1655.

(15) Härth M, Schubert DW. Simple approach for spreading dynamics of polymeric fluids. *Macromolecular Chemistry and Physics*. 2012;213:654–665.

(16) Brochard-Wyart F, de Gennes P. Dynamics of partial wetting. *Adv in Colloid and Interface Science*. 1992; 39:1 – 11.

(17) Snoeijer JH, Andreotti B. Moving Contact Lines: Scales, Regimes, and Dynamical Transitions. *Annu Rev Fluid Mechanics*. 2013;45:269–292.

(18) Jansons KM. Moving contact lines at non-zero capillary number. *J Fluid Mech.* 1986; 167:393–407.

(19) Dussan VEB, Ramé E, Garoff S. On identifying the appropriate boundary conditions at a moving contact line: an experimental investigation. *J Fluid Mech.* 1991; 230:97–116.

(20) Eddi A, Winkels KG, Snoeijer JH. Short time dynamics of viscous drop spreading. *Phys Fluids*. 2013; 25:013102.

(21) Szekely J, Neumann A, Chuang Y. The rate of capillary penetration and the applicability of the Washburn equation. *J Colloid and Interface Science*. 1971; 35:273 – 278.

(22) Ichikawa N, Satoda Y. Interface dynamics of capillary flow in a tube under negligible gravity condition. *J Colloid and Interface Science*. 1994; 162:350 – 355.

(23) Zhmud B, Tiberg F, Hallstensson K. Dynamics of capillary rise. *J Colloid and Interface Science*. 2000; 228:263–269.

(24) Courbin L, Denieul E, Dressaire E, Roper M, Ajdari A, Stone HA. Imbibition by polygonal spreading on microdecorated surfaces. *Nature Materials*. 2007; 6:661–664.

(25) Stauffer CE. The measurement of surface tension by the pendant drop technique. *J Phys Chem*. 1965; 69:1933–1938.

(26) Fujii H, Nakae H. Effect of gravity on contact angle. *Philosophical Magazine A*. 1995; 72:1505–1512.